Multiple myeloma exhibits novel dependence on GLUT4, GLUT8, and GLUT11: implications for glucose transporter-directed therapy

Samuel K. McBrayer,[1] Javelin C. Cheng,[1] Seema Singhal,[1,2] Nancy L. Krett,[1] Steven T. Rosen,[1,2] and Mala Shanmugam[1]

Divisions of [1]Hematology and [2]Oncology, Robert H. Lurie Comprehensive Cancer Center, Feinberg School of Medicine, Northwestern University, Chicago, IL

Multiple myeloma is one of numerous malignancies characterized by increased glucose consumption, a phenomenon with significant prognostic implications in this disease. Few studies have focused on elucidating the molecular underpinnings of glucose transporter (GLUT) activation in cancer, knowledge that could facilitate identification of promising therapeutic targets. To address this issue, we performed gene expression profiling studies involving myeloma cell lines and primary cells as well as normal lymphocytes to uncover deregulated GLUT family members in myeloma. Our data demonstrate that myeloma cells exhibit reliance on constitutively cell surface-localized GLUT4 for basal glucose consumption, maintenance of Mcl-1 expression, growth, and survival. We also establish that the activities of the enigmatic transporters GLUT8 and GLUT11 are required for proliferation and viability in myeloma, albeit because of functionalities probably distinct from whole-cell glucose supply. As proof of principle regarding the therapeutic potential of GLUT-targeted compounds, we include evidence of the anti-myeloma effects elicited against both cell lines and primary cells by the FDA-approved HIV protease inhibitor ritonavir, which exerts a selective off-target inhibitory effect on GLUT4. Our work reveals critical roles for novel GLUT family members and highlights a therapeutic strategy entailing selective GLUT inhibition to specifically target aberrant glucose metabolism in cancer. (*Blood*. 2012;119(20): 4686-4697)

Introduction

Multiple myeloma (MM) is a uniformly fatal plasma cell malignancy that accounts for 20% of deaths from all hematologic cancers.[1,2] The molecular pathology of myeloma involves substantial heterogeneity, including hyperdiploidy and/or aberrant chromosomal translocation events; therefore, new therapeutic strategies that are active in advanced disease and target common molecular processes between the distinct molecular subtypes of MM are attractive. One broadly applicable feature of this disease entails an increased avidity for glucose, the phenomenon which forms the basis for ^{18}fluorodeoxyglucose positron emission tomography (FDG-PET). This imaging modality has recently been shown to provide highly valuable prognostic and diagnostic information in large independent clinical myeloma studies. Zamagni et al reported that 76% of 192 myeloma patients presented with PET-positive disease at the time of initial diagnosis,[3] highlighting the early and widespread transition to a hypermetabolic state during myelomagenesis. More importantly perhaps, this study revealed that incomplete suppression of metabolic activity and FDG uptake after autologous stem cell transplantation is strongly associated with inferior progression-free and overall survival rates. Another study of 239 previously untreated MM patients found prognostic implications linked to the extent of tumor FDG uptake: patients with bone lesions exhibiting maximum standardized uptake values greater than 3.9 demonstrated poor event-free survival.[4] Furthermore, patients with at least 3 PET-positive focal lesions had 30-month event-free survival rates of only 66% (vs 87% for those beneath this threshold). These clinical data define the prevalence of elevated metabolic activity in high-risk MM cases and suggest that therapeutic inhibition of glucose metabolism may be an ideal strategy to treat advanced myeloma disease. In vitro studies have shown that glucose metabolism preserves cellular viability through regulation of key apoptotic effectors, such as Bad,[5] Mcl-1,[6] Puma, Noxa, Bim,[7] and Bax.[5,6,8] Bioinformatic analysis of gene expression patterns in lymphoid malignancies confirms the overexpression of numerous enzymes within the glycolytic pathway,[9] suggesting that FDG-PET positivity manifests because of broad alterations at the molecular level.

The feasibility of glucose metabolism-targeted therapeutic strategies, however, has been cast into doubt by clinical failures of the hexokinase inhibitors 2-deoxyglucose and lonidamine. A recent phase 1 trial of 2-deoxyglucose resulted in dose-limiting toxicities at levels far below those required to elicit antitumor activity in mouse models,[10,11] whereas lonidamine has yielded superior tolerability but disappointing efficacy.[12] Intriguingly, the poor efficacy of these compounds may be explained by recent observations suggesting that glucose transport may occupy the primary rate-determining step of glycolysis in malignant cells.[13,14] Therefore, further investigation into the molecular mechanisms underlying enhanced glucose transport rates in cancer is warranted.

The human GLUT gene family (solute carrier family 2A [*SLC2A*]) consists of 14 members encoding integral membrane proteins capable of ATP-independent, facilitative hexose transport. Individual isoforms differ substantially in critical parameters of functionality, including subcellular localization, substrate recognition, and transport kinetics. Although numerous studies correlate the presence of the Warburg effect in solid tumors with GLUT1 overexpression,[15] few functional, comprehensive analyses of the GLUT repertoire in distinct malignancies have been performed.

Submitted September 7, 2011; accepted March 17, 2012. Prepublished online as *Blood* First Edition paper, March 27, 2012; DOI 10.1182/blood-2011-09-377846.

The online version of this article contains a data supplement.

The publication costs of this article were defrayed in part by page charge payment. Therefore, and solely to indicate this fact, this article is hereby marked "advertisement" in accordance with 18 USC section 1734.

Given the clinical relevance of enhanced glucose transport to myeloma pathogenesis and patient prognosis, we undertook an unbiased gene expression screen of the GLUT gene family coupled with extensive functional analyses to reveal the unanticipated dependence of myeloma cells on the activities of GLUT4, GLUT8, and GLUT11.

Methods

Cell culture

The MM.1S cell line was developed in our laboratory. RPMI 8226 and U266 cell lines were obtained from ATCC. All other MM cell lines were graciously provided by Dr Michael Kuehl (National Cancer Institute). INA6 cells were provided with permission from Dr Renate Burger (Division of Stem Cell Transplantation and Immunotherapy, University Medical Center, Kiel, Germany) and were cultured in the presence of IL-6. All cells were cultured in complete RPMI 1640 (Invitrogen) supplemented with 10% FBS, 2mM glutamine, 100 U/mL penicillin, 100 mg/mL streptomycin, 2.5 μg/mL fungizone, and 0.5 μg/mL plasmocin (InvivoGen) and maintained in a 37°C incubator with 5% CO_2. For glucose deprivation experiments, cells were cultured in glucose-free medium supplemented with dialyzed 10% FBS (Invitrogen) and the indicated concentrations of glucose were added.

Isolation of primary myeloma cells and NBL

Approval for collection of all primary cells was obtained from the Institutional Review Board of Northwestern University. Patients provided written informed consent in all cases at time of enrollment in accordance with the Declaration of Helsinki. Mononuclear cells were isolated with Ficoll/Histopaque 1077 (Sigma-Aldrich). An AutoMacs cell sorter (Miltenyi Biotec) was used to purify $CD138^+$ cells from MM patient bone marrow aspirates. Normal B lymphocytes (NBLs) were purified from peripheral blood mononuclear cells (PBMCs) using a negative selection kit (StemCell Technologies).

In vitro B lymphocyte activation

Purified B lymphocytes were incubated with 10 μg/mL anti–human IgM $F(ab')_2$ antibody fragments (Jackson ImmunoResearch Laboratories) under standard culture conditions. Growth assays were performed during each activation experiment to ensure that a proliferative response was observed.

Chemicals and reagents

Standard chemicals, including G418, puromycin, and phloretin, were purchased from Sigma-Aldrich. Antibodies to GLUT1, GLUT4, and Na^+/K^+ ATPase were purchased from Abcam. Antibodies to pAkt, Akt, pPKC-Ser660, pPKC-Thr440, PKCδ, pGSK3, GSK3β, Puma, pBad, Bim, Bid, Bax, p4EBP, and Bcl-xL were from Cell Signaling Technology. Antibodies to Mcl-1, Bok, and Bcl-2 were from Santa Cruz Biotechnology. Antibodies to PARP, GAPDH, and Noxa were from BD Biosciences, Millipore, and ProSci, respectively. Noncommercial antisera were generously provided by these investigators: human GLUT4 by Dr S. Cushman (National Institute of Diabetes and Digestive and Kidney Diseases, Bethesda, MD), mouse GLUT8 by Dr K. Moley (Washington University, St Louis, MO), and human GLUT11 by Dr A. Schürmann (German Institute of Human Nutrition, Potsdam-Rehbrücke, Germany). Ritonavir was purchased from Selleck Chemicals. Doxorubicin was purchased from PolyMed Therapeutics. PP242 was purchased from Chemdea.

Cell growth, proliferation, and death assays

CellTiter 96 AQ_{ueous} Non-Radioactive Cell Proliferation Assay (Promega) was used to determine cell growth according to the manufacturer's instructions. Cell proliferation and viability were quantified using a Beckman Coulter ViCell automated cell viability analyzer. Annexin V/4,6-diamidino-2-phenylindole (DAPI) staining was used to assess cell death via flow cytometry with a Dako CyAn ADP analyzer.

Glucose consumption and lactate production assays

Rates of glucose uptake and lactate extrusion were determined using the Amplex Red Glucose/Glucose Oxidase kit (Invitrogen). For lactate measurements, glucose oxidase was substituted with lactate oxidase (Sigma-Aldrich). Concentrations of each metabolite were measured in media samples taken at the beginning and end of each experiment.

2-NBDG uptake assay

The fluorescent glucose analog 2-NBDG was purchased from Invitrogen. B lymphocytes were washed and resuspended in Krebs-Ringer buffer containing 0.5% BSA. Cells were preincubated (or not) for 10 minutes with 100μM phloretin at 37°C. 2-NBDG was added at a final concentration of 200μM, and the uptake proceeded for 10 minutes at 37°C. Uptake was stopped by the addition of ice-cold PBS. Cells were washed in ice-cold PBS and maintained on ice until flow cytometric analysis on a Dako CyAn ADP analyzer. Background fluorescence intensity of untreated cells was subtracted from mean fluorescence intensity values. DAPI costaining was used to gate on live cells.

Cell fractionation and plasma membrane isolation

A total of 50×10^6 myeloma cells or PBMCs were homogenized using a QIAGEN Tissuelyser LT. Plasma membrane and cytosolic protein fractions were extracted and purified using the BioVision Membrane Protein Extraction Kit according to the manufacturer's instructions.

Immunoblot analysis

Whole cell lysates were prepared with the Complete Lysis-M buffer (Roche Applied Science) supplemented with phosphatase inhibitor cocktail tablets (Roche Applied Science). Immunoblotting was carried out according to a standard protocol with horseradish peroxidase–linked secondary antibodies (Cell Signaling Technology).

RNA extraction and real-time RT-PCR

RNA isolation was performed using the RNeasy Mini Kit (QIAGEN). Primer-probe sets recognizing GLUTs 1 to 12 and Mcl-1 cDNAs were purchased from Applied Biosystems. Primer-probe sets recognizing 3 cDNAs used as loading controls (YWHAZ, RPL13A, and EIF4A2) were purchased from Primerdesign. Loading normalization was performed according to the geNorm method.[16] Additional information on primer-probe sets used in gene expression assays is included in supplemental Methods (available on the *Blood* Web site; see the Supplemental Materials link at the top of the online article).

Immunofluorescence microscopy

Cells were washed in PBS and spun onto microscope slides (Shandon Cytoslide) using a Shandon Cytospin centrifuge (Thermo Fischer Scientific). Slides were fixed in 4% freshly prepared paraformaldehyde at pH 7.4, permeabilized with 0.03% saponin in PBS, and incubated with blocking buffer (10% normal goat serum containing 0.03% saponin). Cells were stained with optimized dilutions of primary and secondary antibodies in blocking buffer for 1 hour at room temperature. Secondary antibodies used for detection were anti–rabbit IgG-Alexa Fluor-568 or -594 or anti–mouse IgG-AlexaFluor-488 (Invitrogen). Cells were mounted with Ultra Cruz mounting medium (Santa Cruz Biotechnology) containing DAPI for counterstaining. Cells were visualized at 63× (1.4 NA) oil objective with an LSM-510 Meta, Carl Zeiss confocal microscope. Image analysis was performed using the Zeiss Axiovision LE image browser.

DNA constructs and cloning

All shRNAs used were in the pLKO.1 lentiviral vector. Additional information on specific GLUT-targeting shRNA sequences is included in

Table 1. Microarray analyses of myeloma patient samples confirm down-regulation of GLUT3 and up-regulation of GLUT8 and GLUT11

Isoform	Study title*	Probe set ID	Fold change	*P*†	Samples compared‡
GLUT3	Zhan myeloma	M20681_at	−3.219	2.13×10^{-10}	MM (74) vs normal PCs from tonsil (7) and bone marrow (37)
GLUT3	Zhan myeloma 3	202498_s_at	−2.36	3.00×10^{-03}	Smoldering MM (12) vs normal PCs from bone marrow (22)
GLUT3	Zhan myeloma 3	202499_s_at	−2.125	.015	Smoldering MM (12) vs normal PCs from bone marrow (22)
GLUT8	Zhan myeloma 3	239426_at	1.382	.05	Smoldering MM (12) vs normal PCs from bone marrow (22)
GLUT11	Mattioli myeloma	221262_s_at	1.855	3.00×10^{-03}	MM (39) vs MGUS (7) and plasma cell leukemia (6)
GLUT11	Mulligan myeloma	221262_s_at	1.565	5.95×10^{-03}	MM patients: dexamethasone nonresponders (42) vs responders (28)
GLUT1	Zhan myeloma 3	201250_s_at	1.858	5.87×10^{-04}	Smoldering MM (12) vs normal PCs from bone marrow (22)
GLUT1	Zhan myeloma 3	201249_at	−1.000	.5	Smoldering MM (12) vs normal PCs from bone marrow (22)

PCs indicates plasma cells; and MGUS, monoclonal gammopathy of undetermined significance.
*Oncomine (Compendia Bioscience) was used for analysis and visualization.
†*P* values are from Oncomine where possible or represent results of 1-tailed, unpaired *t* tests between 2 clinical groups where values are not available.
‡Numbers in parentheses represent the number of samples in each clinical group.

supplemental Methods. GLUT1, $p16^{INK4A}$, and GFP cDNAs were purchased in the lentiviral vector pReceiver-Lv151 from GeneCopoeia. Mcl-1 WT and Mcl-1 5K cDNAs were a gift from Dr Navdeep Chandel (Northwestern University, Chicago, IL) and were cloned into the lentiviral vector pLVX-IRES-Neo (Clontech).

Lentiviral production and myeloma cell transduction

Large-scale production of high-titer lentiviral vectors was carried out according to an established protocol.[17] For transduction, myeloma cells were plated in serum-free medium containing polybrene and centrifuged at 1500*g* for 90 minutes at room temperature.

Bioinformatics analysis of GLUT gene expression profiles in primary myeloma cells

All studies involving microarray analyses of myeloma patient samples and various control samples deposited in the Oncomine database were interrogated for data regarding expression of GLUT1, GLUT3, GLUT4, GLUT8, and GLUT11. Results are shown in Table 1.

Statistical analysis

The number of independent experiments represented by each data figure is indicated in the figure legends. One-sample and 2-sample (paired and unpaired) Student *t* tests were used to calculate 1- or 2-tailed *P* values using GraphPad Prism 5 software. *P* values less than .05 were considered to be statistically significant.

Results

Myeloma cells are dependent on glucose availability

To examine whether FDG-PET positivity observed clinically in myeloma translates to our in vitro disease model, we compared the glucose consumption rates of normal PBMCs with 9 myeloma cell lines (supplemental Figure 1A-B) and affirmed that MM cells exhibit increased glucose avidity in culture as well. Next, we sought to determine whether elevated glucose uptake translates to metabolic dependency on this substrate and subjected 4 myeloma cell lines, NBLs, and primary MM cells to glucose deprivation and assessed the impact on cellular viability (Figure 1A; supplemental Figure 1C). These conditions highlight a stark contrast between normal and malignant lymphocytes, as 4 of the 5 myeloma cells tested exhibited significant apoptosis after glucose-free culture, whereas the viability of normal B cells was not impacted. Although the JJN3 cell line is resistant to the cytotoxic effects of glucose restriction, these cells as well as KMS11, L363, and U266 cells display glucose concentration-dependent proliferation (Figure 1B). Given the association between high-risk MM cases and high FDG uptake, we tested whether the refractory U266 cell line could be sensitized to doxorubicin by sublethal glucose starvation (Figure 1C). Indeed, U266 cells display significantly greater sensitivity to doxorubicin under glucose-limiting conditions. Importantly, the chemosensitizing effect of glucose metabolism inhibition appears to be tumor cell-specific, as a comparable response was not observed in PBMCs (Figure 1D).

MM cell lines overexpress GLUT4, GLUT8, and GLUT11

Recent reports demonstrating that glycolytic flux control in tumor cells resides proximally within the pathway led us to hypothesize that glucose transporter deregulation may be necessary to support the hypermetabolic phenotype observed in MM.[13,14] Therefore, we established an unbiased real-time RT-PCR–based screen to determine relative expression levels of GLUTs 1 to 12 in 9 MM cell lines and NBLs (Figure 1E). To avoid bias, myeloma lines were selected to broadly cover different genotypic disease subtypes.[18] Two GLUT family members were excluded based on evidence that GLUT14 exhibits exclusive expression in the testis and that GLUT13 functions as a proton-coupled *myo*-inositol transporter.[19,20] Our results demonstrate up-regulation of GLUT4, GLUT8, and GLUT11 mRNAs in all cell lines tested relative to normal controls. RNAi-mediated silencing confirmed specificity of the primer-probe sets used (see Figure 4G; supplemental Figure 1F-G). Interestingly, we observe only one case of GLUT1 overexpression (RPMI 8226) and widespread down-regulation of GLUT3.

Primary MM cells exhibit overexpression of GLUT8 and GLUT11

To establish the clinical significance of these findings, we queried microarray studies involving primary myeloma cells deposited in the Oncomine database for GLUTs 1, 3, 4, 8, and 11 (Table 1). Consistent with our PCR data, MM patient samples exhibit up-regulation of GLUT8 and GLUT11 and reduced expression of

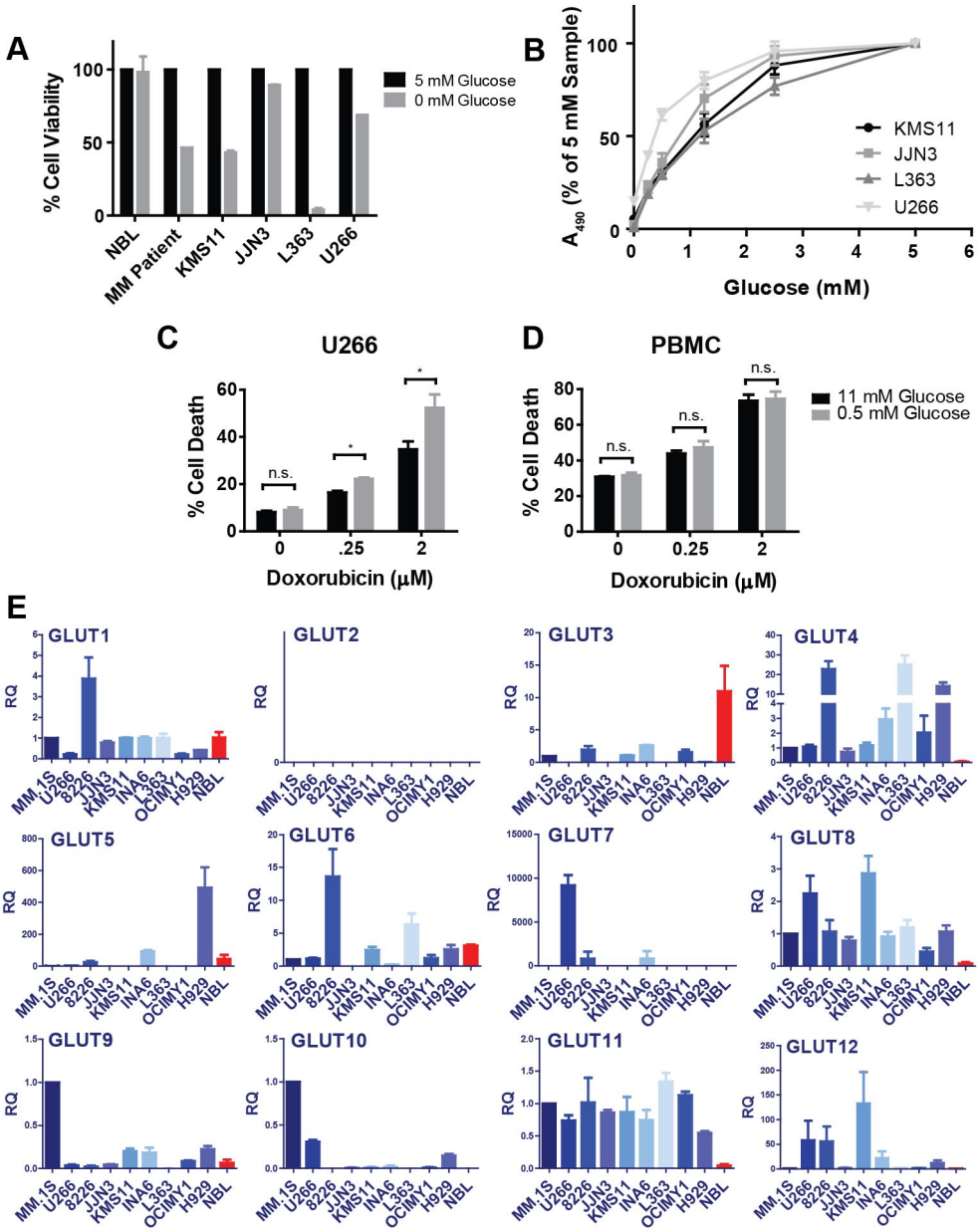

Figure 1. Myeloma cells exhibit glucose dependence and overexpression of GLUT4, GLUT8, and GLUT11 mRNAs relative to NBLs. (A) Primary myeloma cells, NBLs, and 4 MM cell lines were cultured in medium containing 0 or 5mM glucose for 48 (NBL, MM cell lines) or 72 (MM patient) hours. Cell viability was determined by flow cytometric analysis of annexin V/DAPI staining and normalized to 5mM samples. Data are mean ± SEM (n = 2 for MM cell lines and NBL, n = 1 for MM patient sample). (B) MM cell lines were cultured in various glucose concentrations for 72 hours. Viable cell quantities were determined by MTS assay (represented by absorbance at 490 nm) and normalized to 5mM samples. U266 cells (C) and normal PBMCs (D) were cultured in 11 or 0.5mM glucose-containing medium for 48 hours in the presence of the indicated concentrations of doxorubicin. Cell death was determined by DAPI staining. (E) Expression of GLUTs 1 to 12 was determined in 9 myeloma cell lines and NBLs (red bars) by quantitative real-time RT-PCR. Relative quantification (RQ) is displayed and normalized to the MM.1S cell line. For GLUT4, GLUT8, and GLUT11, comparisons between each MM cell line and NBLs exhibit 1-tailed *P* values less than .05, with the exception of GLUT4 expression in the OCIMY1 cell line. (B-E) Data are mean ± SEM (n ≥ 3). **P* < .05. ***P* < .01. ****P* < .005.

GLUT3 relative to normal plasma cells. In contrast to our PCR results, we found no evidence for GLUT4 overexpression. Only 1 study demonstrated differential GLUT1 expression; however, this was dependent on the specific probe set used. To further explore discrepancies related to GLUT1 and GLUT4, we performed immunoblot analyses to evaluate protein expression. GLUT1 protein expression correlates tightly with mRNA levels, supporting the conclusion that GLUT1 expression is not significantly impacted during myelomagenesis (supplemental Figure 1D). GLUT4 protein content is modestly elevated in approximately half of the cell lines interrogated (supplemental Figure 1E). Given this variable overexpression and the potential for extensive posttranslational regulation of GLUT4 via trafficking, we selected GLUT4 together with GLUT8 and GLUT11 for more rigorous functional evaluation. GLUT1 was also included as a standard of comparison because of its presumed role in the pathobiology of many solid tumors.

GLUT4 activity is required for myeloma growth and viability

Transduction of 3 MM cell lines with a GLUT4-targeted shRNA resulted in potent suppression of GLUT4 expression, glucose

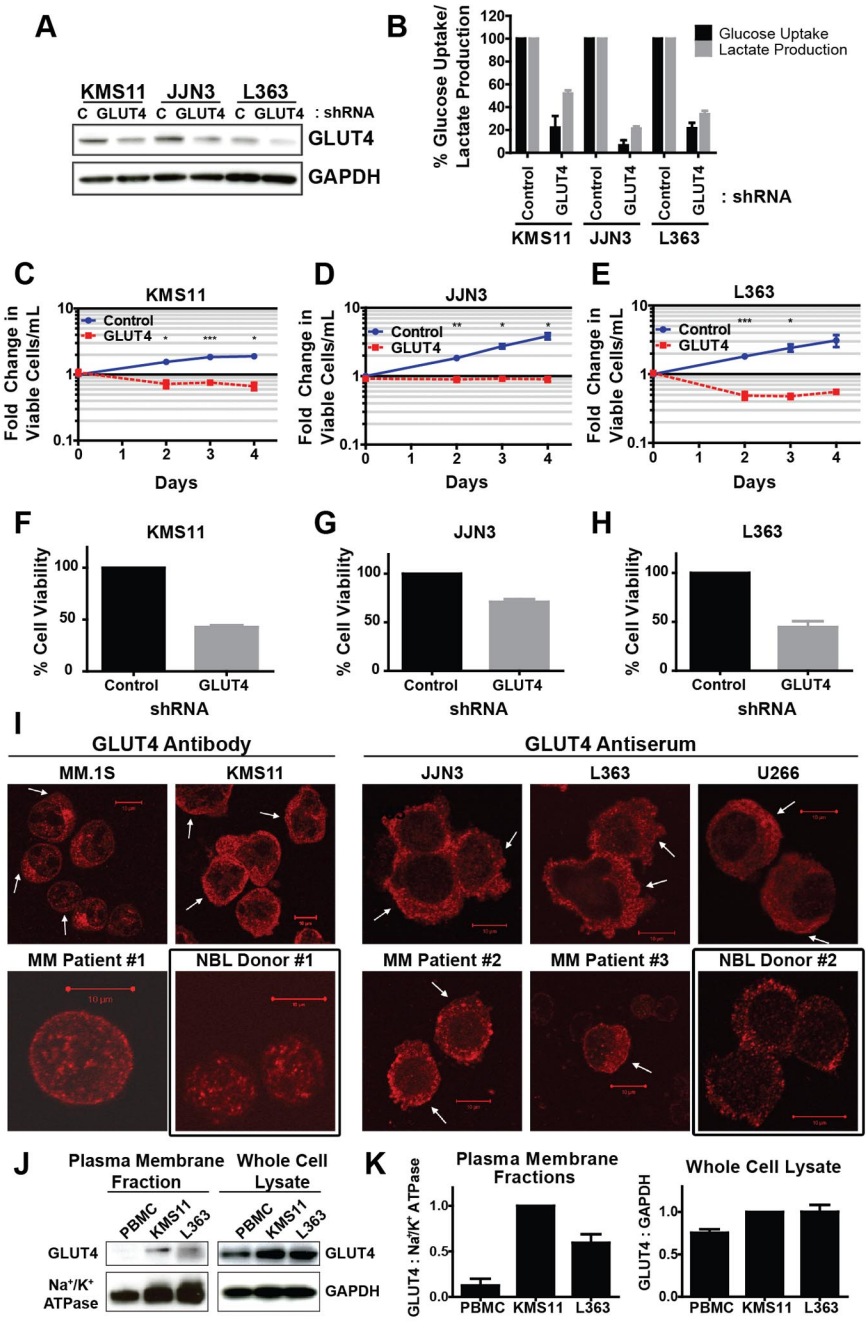

Figure 2. Expression of constitutively plasma membrane-localized GLUT4 is necessary for glucose consumption, lactate production, growth, and viability of myeloma cells. (A) Cells were transduced with control (C), nontargeted shRNA or GLUT4-targeted shRNA and incubated 3 (L363) or 4 (JJN3, KMS11) days before protein extraction, and analysis of GLUT4 protein expression was performed. Representative blot is shown. (B) Cells from panel A were cultured in 5mM glucose-containing medium for 5 hours. Glucose consumption rates and lactate production rates were determined and normalized to control shRNA-expressing cells. (C-E) Cells from panel A were analyzed for viability and proliferation. Viable cell densities are expressed as fold change relative to the day 0 reading of control shRNA-expressing cells. (F-H) Cells from panels C through E were evaluated for viability via trypan blue exclusion. Values are normalized to control shRNA-expressing cells. (I) GLUT4 localization in $CD138^+$ primary myeloma cells, myeloma cell lines, and NBLs was assessed via confocal immunofluorescence microscopy. Arrows indicate regions of cell surface GLUT4 immunoreactivity. Black boxes represent normal controls. Representative images are shown ($n = 1$ for primary samples). (J) KMS11 cells, L363 cells, and normal PBMCs were lysed for extraction of plasma membrane-associated proteins or total cellular protein content. GLUT4 immunoblot analysis was performed on the resulting fractions. Na^+/K^+ ATPase and GAPDH serve as loading controls. (K) Densitometric quantification of band intensities in panel G are displayed, normalized first to corresponding loading controls and subsequently to KMS11 cells. (B-H,K) Data are mean ± SEM. With exception noted in panel I, $n \geq 3$ for data in panels A through K. $^*P < .05$. $^{**}P < .01$. $^{***}P < .005$.

consumption, and lactate production, suggesting that GLUT4 activity is critical for maintaining glycolytic flux (Figure 2A-B). These effects were associated with cytotoxic outcomes in KMS11 and L363 cells and complete cytostasis in JJN3 cells (Figure 2C-H). Importantly, these GLUT4 silencing phenotypes faithfully recapitulate the impact of glucose deprivation in these cell lines; only JJN3 cells are resistant to apoptosis during short-term glucose starvation, but all 3 lines exhibit growth arrest (Figure 1A-B). Expression of an alternative GLUT4 shRNA supports specificity of the RNAi approach (supplemental Figure 2K-L). To place these findings in context, more modest effects on glucose uptake, proliferation, and cell viability are observed after GLUT1 suppression (supplemental Figure 3A-H). Taken together, these data reveal a greater reliance on GLUT4 activity versus that of GLUT1 for maintenance of basal glucose supply in myeloma cells.

MM cells exhibit basal cell surface localization of GLUT4

Canonical GLUT4 activation involves a rise in plasma insulin concentrations; the transporter is rendered inactive under basal conditions through intracellular retention but translocates to the plasma membrane in response to insulin receptor signaling. We reasoned that the basal dependence of MM cells on this transporter may be the result of constitutive trafficking of GLUT4 to the cell surface. To test this hypothesis, we used confocal immunofluorescence microscopy to evaluate the subcellular distribution of GLUT4 and GLUT1 (Figure 2I; supplemental Figures 2A-J and 3I-K). Analysis of myeloma cell lines and patient samples revealed a GLUT4 localization pattern consistent with constitutive activation: all samples tested displayed partial localization of the transporter at the cell surface. In contrast, the GLUT4 pool in NBLs

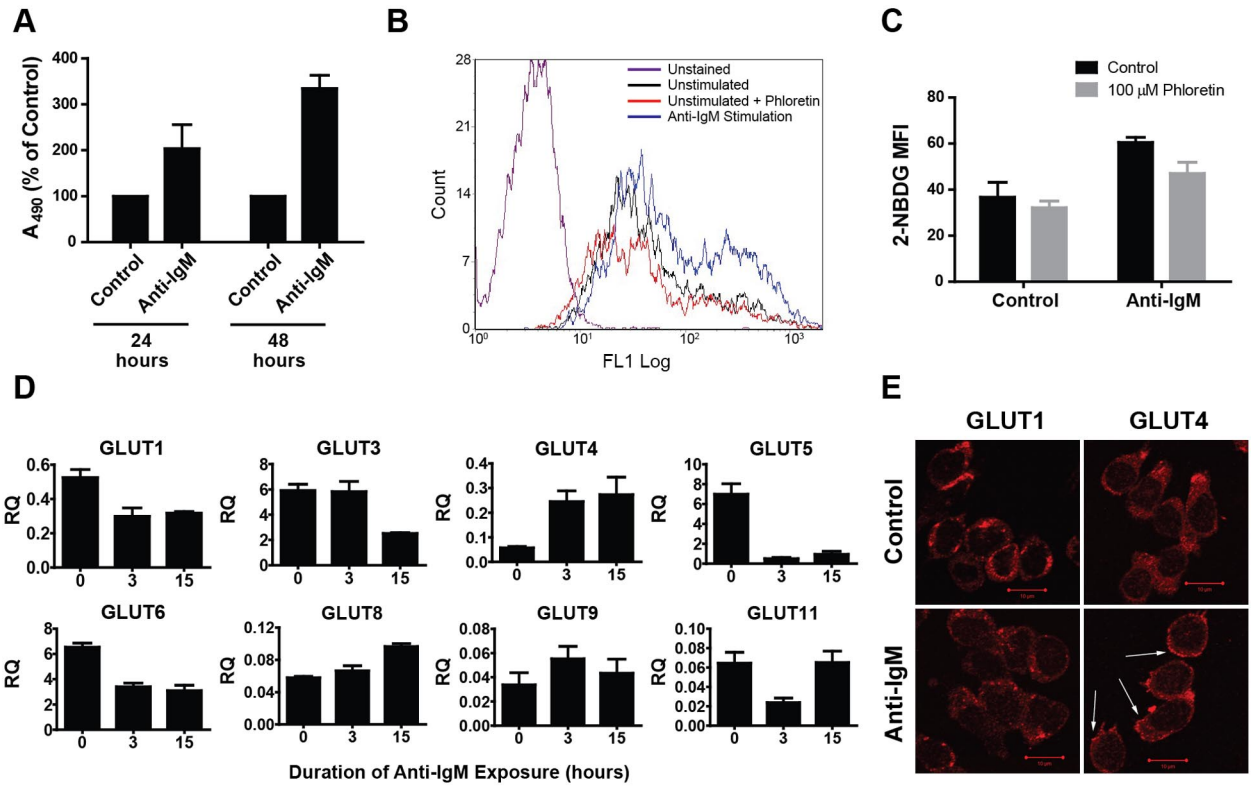

Figure 3. Anti-IgM–mediated B lymphocyte activation is associated with an increase in GLUT4 expression and cell surface localization. (A) NBLs isolated from whole blood were incubated with or without anti–human IgM F(ab′)$_2$ for the indicated durations, and viable cell quantities were determined by MTS assay (represented by absorbance at 490 nm) and normalized to control cells. Data are mean ± SEM (n ≥ 2). (B) NBLs incubated with or without anti-IgM for 15 hours and pretreated (or not) with 100μM phloretin before evaluation of glucose consumption rates via 2-NBDG uptake assay and flow cytometric quantification of fluorescence intensity. A representative histogram is shown. (C) Quantification of data represented in panel B is shown. Median fluorescence intensity values were derived from 3 independent experiments. Data are mean ± SEM (n = 3). (D) Expression of GLUTs 1 to 12 was determined in a time-course analysis of B lymphocytes incubated with anti-IgM for 0, 3, and 15 hours by quantitative real-time RT-PCR. Relative quantification (RQ) is displayed and normalized to the MM.1S cell line for reference to expression levels in myeloma. GLUTs 2, 7, 10, and 12 were undetected. Data are mean ± SEM (n ≥ 2). (E) B lymphocytes were incubated with or without anti-IgM for 15 hours before analysis of GLUT1 and GLUT4 intracellular distribution via confocal immunofluorescence microscopy. Arrows indicate regions of cell surface GLUT4 immunoreactivity. Representative images are shown (n = 4).

appears to reside in an exclusively intracellular compartment based on the punctate cytosolic staining pattern, consistent with the classic paradigm of inducible GLUT4 activation. Subcellular fractionation of PBMCs and KMS11 and L363 cell lines provided quantitative validation of differential GLUT4 distribution (Figure 2J-K). These data suggest a model in which circumvention of GLUT4 intracellular retention mechanisms in MM cells results in constitutive activation of this transporter and elevated rates of glucose uptake (see Figure 6J).

B-cell activation recapitulates basal GLUT4 regulation in myeloma

B lymphocyte activation afterB-cell antigen receptor (BCR) engagement is known to involve a proliferative response[21] and an associated increase in glucose metabolic rate.[22] Therefore, we were interested in elucidating glucose transporter regulation in this normal physiologic context. To mimic antigen-B-cell receptor binding, we incubated cells with anti–human IgM F(ab′)$_2$ fragments to intiate crosslinking. Anti-IgM exposure induced an increase in proliferation (Figure 3A) and glucose consumption (as measured by uptake of the fluorescent glucose analog 2-NBDG, Figure 3B-C). In Figure 3D, real-time RT-PCR analysis of changes in GLUT gene family expression profiles revealed up-regulation of GLUT4 and GLUT8 and a decline in GLUT1 and GLUT3 levels. Assessment of GLUT1 and GLUT4 protein content by immunofluorescence microscopy mirrored the trends seen at the transcriptional level (Figure 3E; supplemental Figure 4). Furthermore, GLUT4 exhibited a striking redistribution to the plasma membrane, reminiscent of the localization of this transporter in myeloma cells. These data suggest that the metabolic response that occurs during B-cell activation may involve GLUT4-mediated glucose transport and that myeloma cells may aberrantly co-opt this mechanism to support the malignant phenotype.

GLUT8 and GLUT11 activities are essential but ambiguous

Given our data supporting GLUT4 as the primary isoform responsible for enhanced glucose consumption rates in MM, we were interested in investigating the functional contributions of GLUT8 and GLUT11. Knockdown of GLUT8 (Figure 4A) resulted in robust cell death induction in KMS11 and L363 cells and growth inhibition with delayed cytotoxicity in the JJN3 background (Figure 4C-E) despite relatively modest inhibition of glucose transport and lactate production rates (Figure 4B). The specificity of the GLUT8 shRNA used was validated by comparison with a second, less efficient shRNA (supplemental Figure 5A-B). In addition to the minor impact on glucose consumption, the exclusively cytoplasmic GLUT8 staining pattern in both myeloma cells and B lymphocytes (Figures 4F and supplemental Figure 5C-E) supports an intracellular role for GLUT8 distinct from that of GLUT1 or GLUT4. However, the observation of any decline in glucose consumption after suppression of a GLUT isoform devoid of plasma membrane localization was perplexing. One potential explanation for this phenomenon lies in the intricate crosstalk

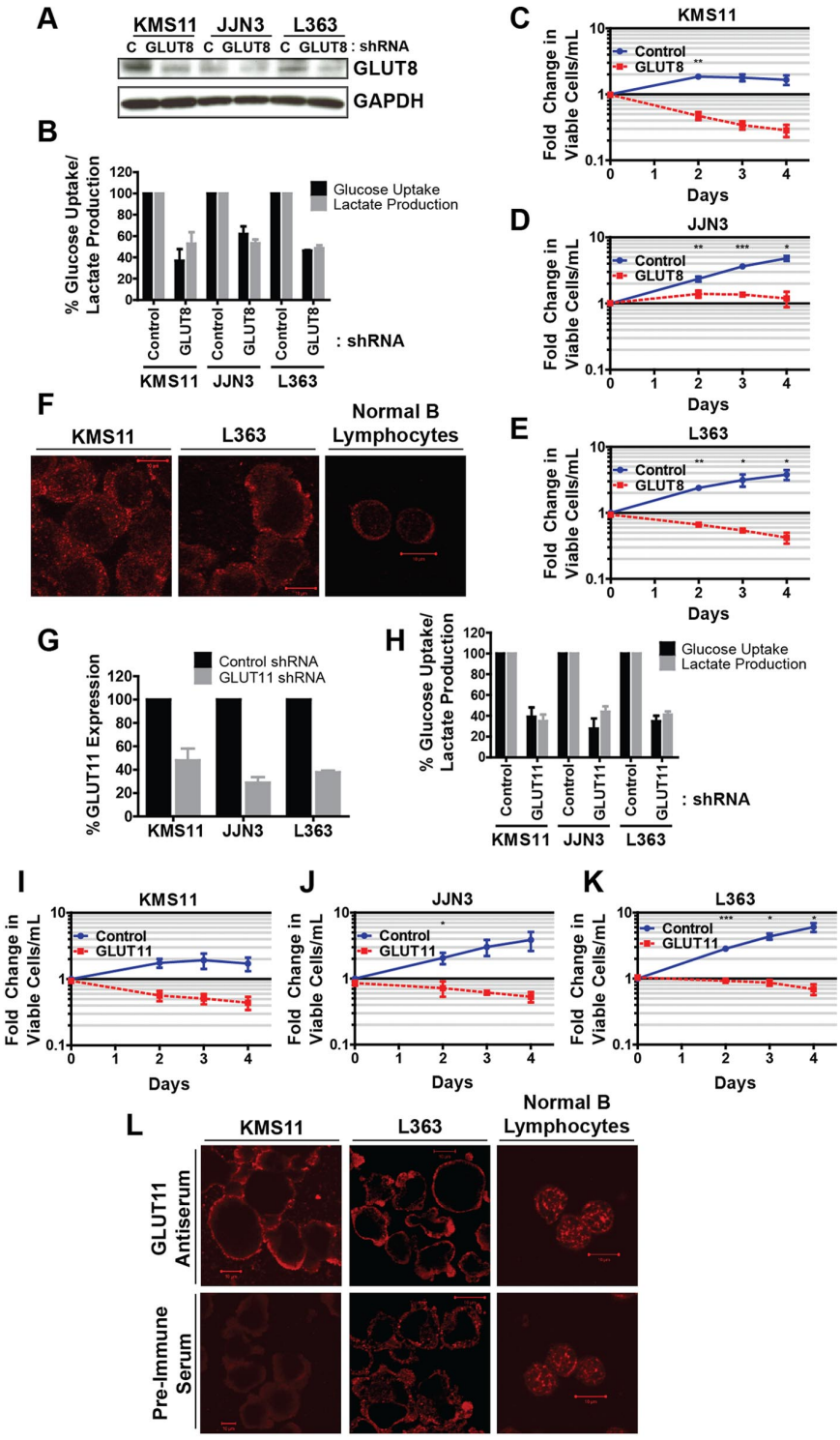

Figure 4. RNAi-mediated suppression of GLUT8 or GLUT11 compromises the viability of myeloma cell lines. (A) Cells were transduced with the indicated shRNAs and incubated 2 days before protein extraction. Representative blot is shown. (B) Cells from panel A were cultured in 5mM glucose-containing medium for 5 hours. Glucose consumption rates and lactate production rates were determined and normalized to control shRNA-expressing cells. (C-E) Cells from panel A were analyzed for viability and proliferation. Viable cell densities are expressed as fold change relative to the day 0 reading of control shRNA-expressing cells. (F) GLUT8 subcellular localization in KMS11 cells, L363 cells, and NBLs was assessed via confocal immunofluorescence microscopy. Representative images are shown. (G) Cells were transduced with the indicated shRNAs and incubated 3 days before RNA extraction. (H) Cells from panel G were cultured in 5mM glucose-containing medium for 5 hours. Glucose consumption rates and lactate production rates were determined and normalized to control shRNA-expressing cells. (I-K) Cells from panel G were analyzed for viability and proliferation. Viable cell densities are expressed as fold change relative to the day 0 reading of control shRNA-expressing cells. (L) GLUT11 subcellular localization in KMS11 cells, L363 cells, and NBLs was assessed via confocal immunofluorescence microscopy. Background, nonspecific staining with preimmune serum is included as a control. Representative images are shown. (B-E,G-K) Data are mean ± SEM. (A-L) $n \geq 3$. $^{*}P < .05$. $^{**}P < .01$. $^{***}P < .005$.

between cell cycle regulatory networks and metabolic pathways.[23,24] We decided to test whether cell cycle arrest could influence glucose metabolism independently of glucose transporter modulation. Taking advantage of the fact that the gene encoding the CDK4 inhibitor $p16^{INK4A}$ is methylated and transcriptionally repressed in MM cell lines,[25] we overexpressed GFP and $p16^{INK4A}$ cDNAs in the KMS11 cell line (supplemental Figure 5F). Ectopic $p16^{INK4A}$ expression resulted in a cytostatic effect and concomitant reduction of glucose transport rates of approximately 40% (supplemental Figure 5G-H). Considering expression of GLUT1, GLUT4, and GLUT8 shRNAs all reduce MM cell growth, these data indicate that the lack of additivity in glucose transport inhibition between these experiments may be the result of a substantial contribution from cell cycle arrest in each case and reinforce our conclusion that the function of GLUT8 is distinct from whole-cell glucose supply.

GLUT11 elimination results in down-regulation of glucose consumption and lactate extrusion rates comparable with that seen

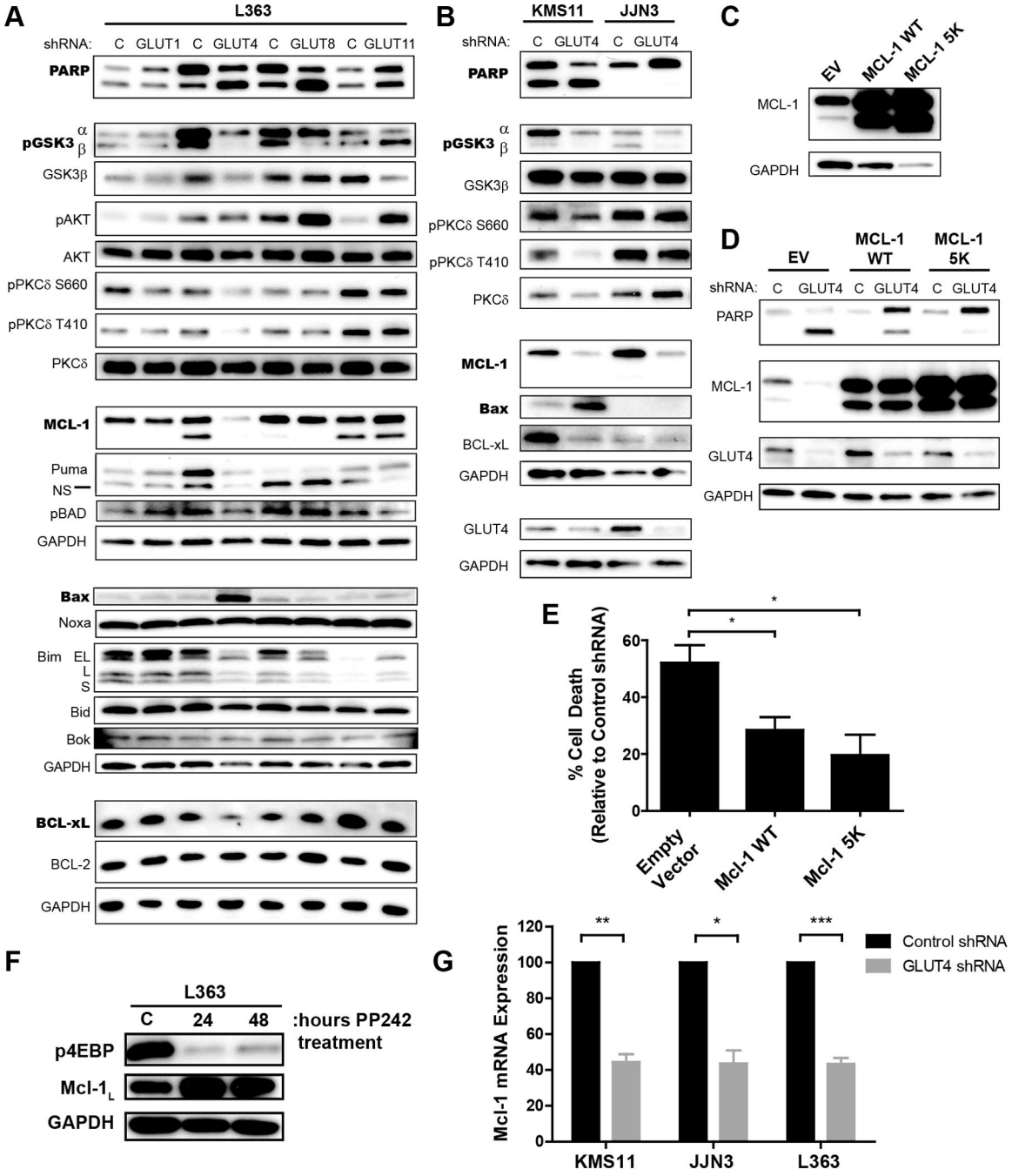

Figure 5. GLUT-specific modulation of signal transducers and apoptosis effectors: cytotoxicity of GLUT4 silencing is mediated by Mcl-1 suppression. (A) L363 cells were transduced with the indicated shRNAs, and cell lysates were prepared. Representative blots are shown. (B) KMS11 and JJN3 cells were transduced with control (C) or GLUT4-targeted shRNA and incubated for 4 days before lysate preparation. Representative blots are shown. (C) L363 cells were transduced with an empty vector control (EV), WT MCL1 (Mcl-1 WT), or ubiquitination-resistant MCL1 mutant (Mcl-1 5K). Stable cell lines were generated, and Mcl-1 expression was assessed by immunoblot analysis. Representative blot is shown. (D) L363 stable cell lines from panel C were transduced with control- or GLUT4-targeted shRNA and incubated for 3 days before immunoblot analysis of GLUT4, Mcl-1, and PARP. Representative blot is shown. (E) Cells from panel D were subjected to flow cytometric viability analysis via annexin V/DAPI staining. Data are normalized to control shRNA-expressing cells within each cell line. Data in panel E are mean ± SEM. (F) L363 cells were treated with DMSO (C) or 1 μM PP242, the active site kinase inhibitor of mTOR, for the indicated lengths of time before protein extraction. Immunoblot analysis of phospho-4EBP1 and Mcl-1 levels is shown. GAPDH serves as a loading control. Representative blot is shown (n = 2). (G) Cells were transduced with control or GLUT4-targeted shRNA and incubated 4 days before RNA extraction, and real-time RT-PCR analysis of Mcl-1 mRNA expression was performed. Relative quantities are shown and normalized to control shRNA-expressing cells. (G) Data are mean ± SEM. (A-E,G) n ≥ 3. *$P < .05$. **$P < .01$. ***$P < .005$.

during GLUT1 suppression (Figure 4G-H). We observed a range of apoptotic effects, ranging from severe (KMS11) to mild (L363; Figure 4I-K). In all cases, cells were unable to proliferate without endogenous GLUT11 activity. Specificity of the RNAi approach was validated through the use of a second GLUT11 shRNA (supplemental Figure 6A-B). Investigation of GLUT11 subcellular localization indicates that it is exclusively associated with the plasma membrane (Figure 4L; supplemental Figure 6C). Furthermore, the differential signal intensity of GLUT11 antiserum versus control, preimmune serum is much greater in MM cells than in B lymphocytes, confirming overexpression at the protein level. It is noteworthy that GLUT11 silencing in JJN3 cells results in less

potent suppression of glucose consumption rates but much greater cytotoxicity relative to GLUT4 knockdown. This phenotypic discordance intimates that the metabolic contributions of GLUT11 may not be entirely encompassed by the glucose transport activity attributed to this protein.

GLUT4 suppression reduces Mcl-1 levels to elicit apoptosis

To elucidate the pathway linking GLUT4 activity with cell survival, we performed immunoblot analyses of key glucose-regulated and apoptosis-related proteins in L363 cells expressing control, GLUT1, GLUT4, GLUT8, and GLUT11 shRNAs (Figure 5A). GLUT4 expression is specifically associated with phosphorylation of protein kinase C δ (PKCδ), glycogen synthase kinase 3 (GSK-3), and Bad, as well as maintenance of Mcl-1 and Bcl-xL levels and suppression of Bax. Evaluation of these effectors in KMS11 and JJN3 cells (Figure 5B) reveals that the only common outcomes of GLUT4 knockdown are GSK-3 dephosphorylation and suppression of Mcl-1. Previous reports have identified Mcl-1 as a substrate for GSK-3β kinase activity and have demonstrated that Mcl-1 undergoes proteasomal degradation after phosphorylation.[26] To determine whether abrogation of Mcl-1 expression was critical for GLUT4 knockdown-induced cell death, we generated L363 stable cell lines expressing an empty vector, a wild-type (WT) *MCL1* cDNA (MCL-1 WT), or an *MCL1* mutant cDNA (MCL-1 5K) encoding a degradation-resistant protein lacking 5 lysine residues necessary for ubiquitination[27] (Figure 5C). GLUT4 silencing in Mcl-1–overexpressing lines results in decreased PARP cleavage and apoptosis compared with cells transduced with empty vector (Figure 5D-E). Interestingly, GLUT4 knockdown did not result in suppression of ectopic WT Mcl-1 expression and the cytoprotection afforded by the 2 *MCL1* constructs correlated with basal Mcl-1 protein abundance. Another putative mechanism accounting for the metabolic regulation of Mcl-1 expression lies in mTOR-dependent translation.[28] However, this association seems unlikely to be relevant in this context given the inability of the mTOR inhibitor PP242 to blunt Mcl-1 expression (Figure 5F). Rather, a decline in Mcl-1 mRNA levels is observed on GLUT4 silencing, pointing to regulation at the transcriptional level as the primary mechanistic linkage (Figure 5G).

Exploiting the GLUT4-inhibitory properties of ritonavir

Serendipitously, certain HIV protease inhibitors elicit off-target inhibitory effects on GLUT4, which are both specific and direct.[29,30] We explored whether the most efficacious member of this drug class, ritonavir (1,3-thiazol-5-ylmethyl N-[(2S,3S,5S)-3-hydroxy-5-[(2S)-3-methyl-2-{[methyl({[2-(propan-2-yl)-1,3-thiazol-4-yl]methyl})carbamoyl]amino}butanamido]-1,6-diphenylhexan-2-yl]carbamate), could yield therapeutically desirable effects against myeloma cells in vitro. As shown in Figure 6A through D, ritonavir treatment elicits dose-dependent abrogation of both glucose transport and proliferation in KMS11 and L363 cells. In addition, ritonavir treatment recapitulates the doxorubicin-sensitizing effects of glucose limitation (supplemental Figure 7A-B). To assess the contribution of glucose transport inhibition to ritonavir-induced growth arrest, we generated KMS11 lines stably expressing *SLC2A1* (GLUT1) or GFP (Figure 6E). Given the specificity of ritonavir for GLUT4, GLUT1 expression completely mitigated ritonavir-induced glucose transport inhibition and simultaneously conferred robust resistance to the growth-inhibitory effects of prolonged treatment (Figure 6F-H). To evaluate the clinical applicability of these findings, we tested ritonavir for cytotoxicity toward primary myeloma cells. In Figure 6A and I, a range of cell death induction is seen in patient samples after incubation with a concentration of ritonavir (20μM), which is approximately equivalent to the peak plasma level routinely achieved in humans.[31] In sum, our results support the model of glucose transporter activity in myeloma represented in Figure 6J and highlight the therapeutic potential of ritonavir-mediated GLUT4 inhibition in this malignancy.

Discussion

Since the seminal discoveries of Otto Warburg nearly a century ago, appreciation of the indispensable role of metabolic adaptation in the process of tumorigenesis has dramatically increased. In particular, the association between glucose metabolism and the maintenance of cellular survival has been firmly established in both normal[8] and malignant[32] contexts. Furthermore, increased glucose consumption serves to supply carbon to various anabolic pathways necessary for biomass duplication preceding mitosis[33] and induces resistance to classic chemotherapeutic agents.[10,34,35] Compelled by evidence that glucose transport may represent the principal rate-determining step of glycolysis in tumor cells,[13,14] we have interrogated the glucose transporter family as a source of novel therapeutic targets. Our data clearly demonstrate myeloma dependence on GLUT4 activity, a phenomenon associated with the basal cell surface localization of the transporter. Constitutive activation of GLUT4 in MM cells contradicts the canonical association between GLUT1 overexpression and the glycolytic phenotype in cancer. Previous work from our group[36] implied the existence of a substantial GLUT1-independent glucose transport activity in myeloma, a concept bolstered by the observation that GLUT1 down-regulation in the OPM2 myeloma cell line results in a modest reduction in 3-*O*-methyl-glucose uptake.[37] Selective mobilization of GLUT4 by myeloma cells may potentially be explained by a detrimental enzyme production cost associated with de novo overexpression of GLUT1.[38] Alternatively, GLUT4 selection may simply be attributable to a higher affinity for glucose: K_M values for 3-*O*-methyl-glucose transport are 4.3mM and 26.2mM for GLUT4 and GLUT1, respectively.[39]

Examination of glucose transporter regulation during B-cell activation revealed similar mobilization of GLUT4 and an associated increase in GLUT4 expression, effects that directly contrast those on GLUT1. These data suggest that GLUT4 activation facilitates increased glycolytic flux observed during human B lymphocyte stimulation and that myeloma cells may exploit this process to achieve a perpetual hypermetabolic state. A similar study of activated murine B cells noted an up-regulation of GLUT1 protein expression.[22] It remains to be explored whether these differences reflect species-specific glucose transporter use by B lymphocytes. Interestingly, this concept has precedence in erythropoiesis: GLUT1 expression is undetectable in mature murine erythrocytes but is potently up-regulated during human red blood cell differentiation.[40] Data from this same study also confirmed the expression of GLUT4 in murine erythrocytes, suggesting that it may be responsible for glucose consumption in this context.

We also report crucial but elusive functionalities of GLUT8 and GLUT11 in myeloma. Our data relating to the intracellular localization of GLUT8 corroborate studies carried out in primary spermatocytes and hippocampal neurons (tissues characterized by high endogenous GLUT8 expression[41,42]). GLUT8 contains a

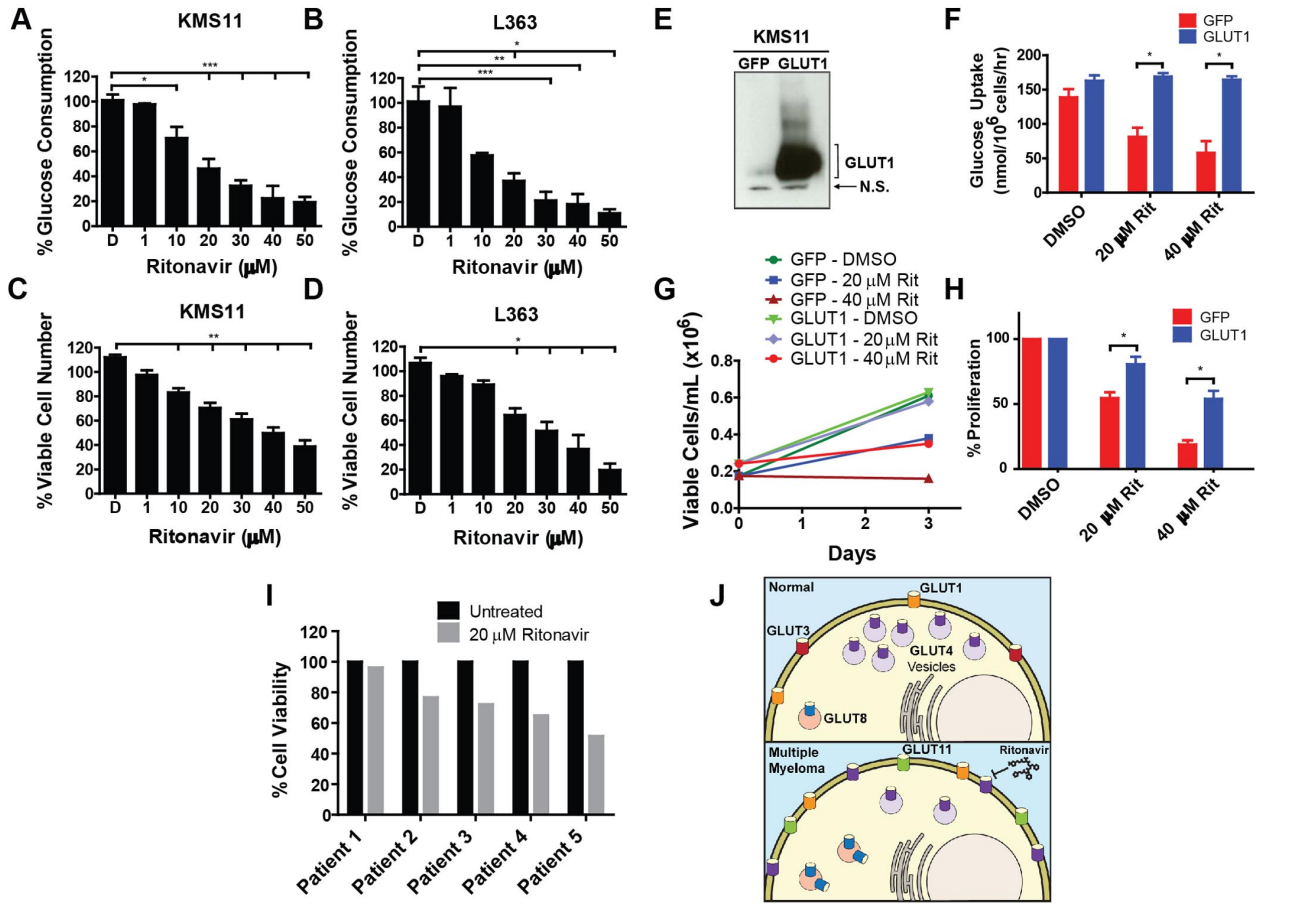

Figure 6. GLUT4-specific glucose transport inhibition elicited by the HIV therapeutic ritonavir suppresses myeloma growth and viability. (A) KMS11 and (B) L363 cells were plated in 5mM glucose medium with ritonavir or DMSO (D) for 17 hours. Glucose consumption rates are normalized to untreated cells (not shown). (C) KMS11 and (D) L363 cells were treated with ritonavir or DMSO for 72 hours. Relative viable cell numbers were determined by MTS assay and normalized to untreated cells (not shown). (E) Stable KMS11 cell lines were generated expressing empty vector or GLUT1 and GLUT1 levels were assessed by immunoblot analysis. Representative blot is shown. N.S. indicates nonspecific band. (F) Stable cell lines from panel E were treated with DMSO or ritonavir (Rit) for 5 hours, and glucose consumption was assessed. (G) Cell proliferation was measured in the stable cell lines described in panel E treated with ritonavir (Rit) or DMSO for 72 hours. A representative experiment is shown. (H) Cell proliferation rates from multiple experiments represented by panel G are normalized to DMSO-treated cells. (I) Primary myeloma cells were treated with DMSO or ritonavir for 72 hours before annexin V/DAPI staining. Values are normalized to DMSO-treated samples (n = 1 for each patient sample). (J) Diagram highlights alterations in glucose transporter regulation between NBLs/plasma cells (top) and MM cells (bottom). (A-D,F,H) Data are mean ± SEM. (A-H) n ≥ 3. *$P < .05$. **$P < .01$. ***$P < .005$.

distinctive [DE]XXXL[LI] amino acid motif not found in either GLUT4 or GLUT1, which directs trafficking to an unspecified late endosomal/lysosomal compartment.[43] Given the association of GLUT8 with known exocytic compartments and the extensive production of immunoglobulin by myeloma cells,[44] we hypothesize that GLUT8 plays a role in facilitating efficient protein secretion. This function would be consistent with the up-regulation of GLUT8 we observe in activated B cells given the increase in antibody production that accompanies this process.

We propose a primary function for GLUT11 involving the cellular supply of a metabolic substrate other than glucose. First, the impact on glucose consumption rates and cytotoxic effects elicited by GLUT11 knockdown in our studies are incongruous. Second, GLUT11 has strikingly low K_M values for both glucose and fructose in relation to other GLUT family members,[45] a prerequisite for transport of low-abundance substrates. Third, GLUT11 localization has been shown to be restricted to the plasma membrane in all studies to date.[46] Fourth, other members of the class II GLUT subfamily exhibit preferential transport of metabolites other than glucose. For example, GLUT5 is principally associated with fructose uptake, whereas GLUT9 has been shown to mediate urate transport.[47]

Our investigation into the connection between GLUT4 activity and MM cell survival delineates a pathway linking GLUT4 activity with the maintenance of Mcl-1 expression. We conclude that Mcl-1 suppression is necessary but not sufficient to cause cell death after GLUT4 inhibition based on the observation that JJN3 cells exhibit reduced Mcl-1 protein levels during GLUT4 knockdown without significant cytotoxicity. Concomitant alteration of Bcl-xL and Bax expression observed only in sensitive cells may provide additional modulation of the apoptotic rheostat necessary for cell death. The mechanistic underpinnings of this GLUT4–Mcl-1 association are independent of proteasomal degradation[6] and mTOR-dependent translation[28] but rather involve regulation of Mcl-1 at the transcriptional level. The ability to target Mcl-1 through GLUT4 inhibition has profound clinical implications because of the inferior prognosis conferred by high Mcl-1 expression in myeloma.[48]

Finally, we have demonstrated that the off-target inhibitory effect on GLUT4 of the HIV protease inhibitor ritonavir can be exploited to reduce myeloma proliferation and viability and increase chemosensitivity. Although the growth-inhibitory properties of ritonavir and related compounds saquinavir and nelfinavir toward myeloma cells have been established,[49] our data demonstrate that these effects stem

from inhibition of GLUT4-dependent glucose consumption. This finding provides strong rationale for the initiation of clinical trials to assess the efficacy of ritonavir in myeloma, a repositioning that could be implemented rapidly given its approval by the FDA. Indeed, ritonavir is currently being tested in several ongoing clinical trials in other malignancies. The widely acknowledged presence of metabolic side effects associated with chronic ritonavir administration (which recapitulate some of the pathologies seen in GLUT4 knockout mice[50]) suggests that GLUT4 activity is impacted by the dosages used in HIV therapy. Although these side effects are also a concern with regard to the use of ritonavir to treat MM, we think that the chronic dosing schedule necessary to prevent HIV replication may not be required to elicit meaningful antimyeloma effects in vivo, and more flexible regimens could ameliorate the adverse metabolic impact of ritonavir on normal tissues. Furthermore, the use of ritonavir in a chemosensitizing role would entail only cyclical administration. We conclude that targeting glucose transport represents a more selective and probably more potent means to leverage the increased metabolic demands associated with tumorigenesis. The development of novel biologics and compounds, which interfere with glucose transporters in an isoform-specific manner, represents a potentially valuable addition to the therapeutic repertoire for the treatment of MM and other glucose-dependent neoplasias.

Acknowledgments

The authors thank Natalie Pulliam for assistance with purification of primary myeloma cells, Jakob Reiser for technical advice relating to lentiviral vector production, and Navdeep Chandel for generously providing the Mcl-1 constructs.

This work was supported by the Northwestern University Cell Imaging Facility and a Cancer Center Support Grant (NCI CA060553), the Robert H. Lurie Comprehensive Cancer Center Flow Cytometry Facility and a Cancer Center Support Grant (NCI CA060553), National Institutes of Health (grant RO1 CA85919, S.T.R.), National Institutes of Health/National Cancer Institute (grant T32CA09560, S.K.M.), American Cancer Society (Illinois Division, grants 140565 and 188679, M.S.), American Cancer Society (Research Scholar grant RSG-11-254-01-CSM, M.S.), and Wendy Will Case Cancer Fund Foundation (grant SP0012544, M.S.).

Authorship

Contribution: S.K.M. and M.S. conceived and performed the research; S.T.R., S.K.M., J.C.C., and M.S. provided conceptual advice; S.S. oversaw collection of myeloma patient samples; S.K.M., J.C.C., N.L.K., S.T.R., and M.S. analyzed data; S.K.M. wrote the manuscript; and M.S. edited the manuscript and supervised the project.

Conflict-of-interest disclosure: The authors declare no competing financial interests.

Correspondence: Mala Shanmugam, Robert H. Lurie Comprehensive Cancer Center, 3-250 Lurie Bldg, Feinberg School of Medicine, Northwestern University, 303 E Superior St, Chicago, IL 60611; e-mail: mala@northwestern.edu.

References

1. Richardson PG, Schlossman R, Hideshima T, Anderson KC. New treatments for multiple myeloma. *Oncology (Williston Park)*. 2005;19(14): 1781-1792; discussion 1792,1795-1787.
2. Munshi N. Plasma cell disorders: an historical perspective. *Hematology.* 2008;1:297.
3. Zamagni E, Patriarca F, Nanni C, et al. Prognostic relevance of 18-F FDG PET/CT in newly diagnosed multiple myeloma patients treated with upfront autologous transplantation. *Blood.* 2011; 118(23):5989-5995.
4. Bartel TB, Haessler J, Brown TL, et al. F18-fluorodeoxyglucose positron emission tomography in the context of other imaging techniques and prognostic factors in multiple myeloma. *Blood.* 2009;114(10):2068-2076.
5. Danial NN, Gramm CF, Scorrano L, et al. BAD and glucokinase reside in a mitochondrial complex that integrates glycolysis and apoptosis. *Nature.* 2003;424(6951):952-956.
6. Zhao Y, Altman BJ, Coloff JL, et al. Glycogen synthase kinase 3alpha and 3beta mediate a glucose-sensitive antiapoptotic signaling pathway to stabilize Mcl-1. *Mol Cell Biol.* 2007;27(12):4328-4339.
7. Coloff JL, Mason EF, Altman BJ, et al. Akt requires glucose metabolism to suppress puma expression and prevent apoptosis of leukemic T cells. *J Biol Chem.* 2011;286(7):5921-5933.
8. Rathmell JC, Fox CJ, Plas DR, Hammerman PS, Cinalli RM, Thompson CB. Akt-directed glucose metabolism can prevent Bax conformation change and promote growth factor-independent survival. *Mol Cell Biol.* 2003;23(20):7315-7328.
9. Altenberg B, Greulich KO. Genes of glycolysis are ubiquitously overexpressed in 24 cancer classes. *Genomics.* 2004;84(6):1014-1020.
10. Maschek G, Savaraj N, Priebe W, et al. 2-deoxy-D-glucose increases the efficacy of adriamycin and paclitaxel in human osteosarcoma and non-small cell lung cancers in vivo. *Cancer Res.* 2004; 64(1):31-34.
11. Raez LE, Langmuir VK, Papadopoulus K, et al. Phase I trial of glycolytic inhibition with 2-deoxyglucose and docetaxel for patients with solid tumors [abstract]. *AACR Meeting Abstracts.* 2006;2006(1):121-d-122. Abstract 515.
12. Berruti A, Bitossi R, Gorzegno G, et al. Time to progression in metastatic breast cancer patients treated with epirubicin is not improved by the addition of either cisplatin or lonidamine: final results of a phase III study with a factorial design. *J Clin Oncol.* 2002;20(20):4150-4159.
13. Rodriguez-Enriquez S, Marin-Hernandez A, Gallardo-Perez JC, Moreno-Sanchez R. Kinetics of transport and phosphorylation of glucose in cancer cells. *J Cell Physiol.* 2009;221(3):552-559.
14. Marin-Hernandez A, Rodriguez-Enriquez S, Vital-Gonzalez PA, et al. Determining and understanding the control of glycolysis in fast-growth tumor cells: flux control by an over-expressed but strongly product-inhibited hexokinase. *FEBS J.* 2006;273(9):1975-1988.
15. Medina RA, Owen GI. Glucose transporters: expression, regulation and cancer. *Biol Res.* 2002; 35(1):9-26.
16. Vandesompele J, De Preter K, Pattyn F, et al. Accurate normalization of real-time quantitative RT-PCR data by geometric averaging of multiple internal control genes. *Genome Biol.* 2002;3(7): RESEARCH0034.
17. Kutner RH, Zhang XY, Reiser J. Production, concentration and titration of pseudotyped HIV-1-based lentiviral vectors. *Nat Protoc.* 2009;4(4): 495-505.
18. Moreaux J, Klein B, Bataille R, et al. A high-risk signature for patients with multiple myeloma established from the molecular classification of human myeloma cell lines. *Haematologica.* 2011; 96(4):574-582.
19. Wu X, Freeze HH. GLUT14, a duplicon of GLUT3, is specifically expressed in testis as alternative splice forms. *Genomics.* 2002;80(6): 553-557.
20. Uldry M, Ibberson M, Horisberger JD, Chatton JY, Riederer BM, Thorens B. Identification of a mammalian H(+)-myo-inositol symporter expressed predominantly in the brain. *EMBO J.* 2001;20(16): 4467-4477.
21. Damdinsuren B, Zhang Y, Khalil A, et al. Single round of antigen receptor signaling programs naive B cells to receive T cell help. *Immunity.* 2010; 32(3):355-366.
22. Doughty CA, Bleiman BF, Wagner DJ, et al. Antigen receptor-mediated changes in glucose metabolism in B lymphocytes: role of phosphatidylinositol 3-kinase signaling in the glycolytic control of growth. *Blood.* 2006;107(11):4458-4465.
23. Aguilar V, Fajas L. Cycling through metabolism. *EMBO Mol Med.* 2010;2(9):338-348.
24. Almeida A, Bolanos JP, Moncada S. E3 ubiquitin ligase APC/C-Cdh1 accounts for the Warburg effect by linking glycolysis to cell proliferation. *Proc Natl Acad Sci U S A.* 2010;107(2):738-741.
25. Urashima M, Teoh G, Ogata A, et al. Characterization of p16(INK4A) expression in multiple myeloma and plasma cell leukemia. *Clin Cancer Res.* 1997;3(11):2173-2179.
26. Ding Q, He X, Hsu JM, et al. Degradation of Mcl-1 by beta-TrCP mediates glycogen synthase kinase 3-induced tumor suppression and chemosensitization. *Mol Cell Biol.* 2007;27(11):4006-4017.
27. Snyder CM, Shroff EH, Liu J, Chandel NS. Nitric

oxide induces cell death by regulating anti–apoptotic BCL-2 family members. *PLoS One.* 2009; 4(9):e7059.

28. Coloff JL, Macintyre AN, Nichols AG, et al. Akt-dependent glucose metabolism promotes mcl-1 synthesis to maintain cell survival and resistance to bcl-2 inhibition. *Cancer Res.* 2011;71(15): 5204-5213.
29. Murata H, Hruz PW, Mueckler M. The mechanism of insulin resistance caused by HIV protease inhibitor therapy. *J Biol Chem.* 2000;275(27): 20251-20254.
30. Vyas AK, Koster JC, Tzekov A, Hruz PW. Effects of the HIV protease inhibitor ritonavir in GLUT4 knockout mice. *J Biol Chem.* 2010;285(47): 36395-36400.
31. Hsu A, Granneman GR, Witt G, et al. Multiple-dose pharmacokinetics of ritonavir in human immunodeficiency virus-infected subjects. *Antimicrob Agents Chemother.* 1997;41(5):898-905.
32. Vaughn AE, Deshmukh M. Glucose metabolism inhibits apoptosis in neurons and cancer cells by redox inactivation of cytochrome c. *Nat Cell Biol.* 2008;10(12):1477-1483.
33. Vander Heiden MG, Cantley LC, Thompson CB. Understanding the Warburg effect: the metabolic requirements of cell proliferation. *Science.* 2009; 324(5930):1029-1033.
34. Cao X, Fang L, Gibbs S, et al. Glucose uptake inhibitor sensitizes cancer cells to daunorubicin and overcomes drug resistance in hypoxia. *Cancer Chemother Pharmacol.* 2007;59(4): 495-505.
35. Xu RH, Pelicano H, Zhou Y, et al. Inhibition of glycolysis in cancer cells: a novel strategy to overcome drug resistance associated with mitochondrial respiratory defect and hypoxia. *Cancer Res.* 2005;65(2):613-621.
36. Shanmugam M, McBrayer SK, Qian J, et al. Targeting glucose consumption and autophagy in myeloma with the novel nucleoside analogue 8-aminoadenosine. *J Biol Chem.* 2009;284(39): 26816-26830.
37. Wardell SE, Ilkayeva OR, Wieman HL, et al. Glucose metabolism as a target of histone deacetylase inhibitors. *Mol Endocrinol.* 2009;23(3):388-401.
38. Molenaar D, van Berlo R, de Ridder D, Teusink B. Shifts in growth strategies reflect tradeoffs in cellular economics. *Mol Syst Biol.* 2009;5:323.
39. Nishimura H, Pallardo FV, Seidner GA, Vannucci S, Simpson IA, Birnbaum MJ. Kinetics of GLUT1 and GLUT4 glucose transporters expressed in Xenopus oocytes. *J Biol Chem.* 1993;268(12):8514-8520.
40. Montel-Hagen A, Kinet S, Manel N, et al. Erythrocyte Glut1 triggers dehydroascorbic acid uptake in mammals unable to synthesize vitamin C. *Cell.* 2008;132(6):1039-1048.
41. Schurmann A, Axer H, Scheepers A, Doege H, Joost HG. The glucose transport facilitator GLUT8 is predominantly associated with the acrosomal region of mature spermatozoa. *Cell Tissue Res.* 2002;307(2):237-242.
42. Ibberson M, Riederer BM, Uldry M, Guhl B, Roth J, Thorens B. Immunolocalization of GLUTX1 in the testis and to specific brain areas and vasopressin-containing neurons. *Endocrinology.* 2002;143(1): 276-284.
43. Augustin R, Riley J, Moley KH. GLUT8 contains a [DE]XXXL[LI] sorting motif and localizes to a late endosomal/lysosomal compartment. *Traffic.* 2005;6(12):1196-1212.
44. Meister S, Schubert U, Neubert K, et al. Extensive immunoglobulin production sensitizes myeloma cells for proteasome inhibition. *Cancer Res.* 2007;67(4):1783-1792.
45. Manolescu AR, Augustin R, Moley K, Cheeseman C. A highly conserved hydrophobic motif in the exofacial vestibule of fructose transporting SLC2A proteins acts as a critical determinant of their substrate selectivity. *Mol Membr Biol.* 2007;24(5):455-463.
46. Scheepers A, Schmidt S, Manolescu A, et al. Characterization of the human SLC2A11 (GLUT11) gene: alternative promoter usage, function, expression, and subcellular distribution of three isoforms, and lack of mouse orthologue. *Mol Membr Biol.* 2005;22(4):339-351.
47. Caulfield MJ, Munroe PB, O'Neill D, et al. SLC2A9 is a high-capacity urate transporter in humans. *PLoS Med.* 2008;5(10):e197.
48. Wuilleme-Toumi S, Robillard N, Gomez P, et al. Mcl-1 is overexpressed in multiple myeloma and associated with relapse and shorter survival. *Leukemia.* 2005;19(7):1248-1252.
49. Ikezoe T, Saito T, Bandobashi K, Yang Y, Koeffler HP, Taguchi H. HIV-1 protease inhibitor induces growth arrest and apoptosis of human multiple myeloma cells via inactivation of signal transducer and activator of transcription 3 and extracellular signal-regulated kinase 1/2. *Mol Cancer Ther.* 2004;3(4):473-479.
50. Stenbit AE, Tsao TS, Li J, et al. GLUT4 heterozygous knockout mice develop muscle insulin resistance and diabetes. *Nat Med.* 1997;3(10):1096-1101.